PCCP

PAPER

View Article Online
View Journal

Cite this: DOI: 10.1039/c7cp06703h

Panchromatic cross-conjugated π-bridge NIR dyes for DSCs†

Yanbing Zhang, ‡[a] Hammad Cheema, ‡[a] Alexander E. London,[b] Amber Morales,[a] Jason D. Azoulay[b] and Jared H. Delcamp *[a]

Received 29th September 2017,
Accepted 22nd December 2017

DOI: 10.1039/c7cp06703h

rsc.li/pccp

Four organic sensitizers incorporating a cross-conjugated cyclopenta[2,1-*b*:3,4-*b*′]dithiophene (CPDT) π-bridge have been synthesized. As a result of molecular engineering, broad high energy bands and red shifted absorption maxima and onset is observed relative to a benchmark analogue (**C218**) using a non-cross-conjugated CPDT π-bridge. The use of a cross-conjugated bridge allows a new strategy for tuning dye energetics and introduction of increased absorption uniformity by adding additional high-energy absorption bands. These dyes show solar-to-electric conversion up to 800 nm with one derivative exceeding the performance of **C218** under identical conditions.

Introduction

Developing renewable energy conversion systems is important since worldwide power consumption is increasing dramatically. Research on dye-sensitized solar cells (DSCs) has been fuelled with the potential for affordable production, excellent tunability of device components and relatively high power conversion efficiencies (PCEs) from organic light absorbing materials.[1–5] DSCs operate by light absorption of a sensitizer which then transfers an electron to an inorganic semiconductor. The electron then traverses an external circuit before being collected at the counter electrode by a redox shuttle, which returns the electron back to the oxidized sensitizer. The sensitizer or dye plays several critical roles in this process concerning efficiency of electron transfers and the breadth of the absorption spectrum used. Recently, **SM315** and **ADEKA-1/LEG-4** based devices have achieved record PCEs of 13.0% and 14.3% for single- and co-sensitized DSC device efficiencies, respectively.[6–9] These exceptionally efficient dyes are designed based on three conjugated structural elements: a donor, a π-bridge and an acceptor (D–π–A). The π-bridge plays the critical role of both allowing the donor and acceptor regions to undergo intramolecular charge transfer (ICT) and to define the initial energy levels of the molecule prior to substituent addition. An appropriate π-bridge should: (1) ensure a minimal optical gap to extend the region where sunlight is converted to electricity,[10–14] (2) allow for properly positioned dye energetics for rapid electron transfers to TiO_2 and from the redox shuttle,[15,16] (3) suppress aggregation which lowers PCEs,[17] and (4) reduce non-productive electron transfers (recombination).[18,19]

Thiophene-based building blocks are ubiquitous π-bridges due to excellent ICT properties and synthetic accessability.[20–24] A thiophene-based π-bridge 4,4-dihexyl-4*H*-cyclopenta[2,1-*b*:3,4-*b*′]dithiophene (Hx_2CPDT) was employed in the design of an exceptionally successful organic dye (**C218**) with a triphenyl amine donor (TPA) and cyanoacrylic acid acceptor (CAA) with a high molar absorptivity, low recombination rate and wide absorption range.[25,26] The dialkylated CPDT bridge has now been incorporated into >125 dyes according to a SciFinder search, yet no conjugated alkene analogues have been evaluated. Herein, we have designed a new series of sensitizers with identical donor and acceptor to **C218** that include a solubilizing cross-conjugated bridgehead olefin substituent (C═CPh) substituent replacing the dialkyl chains on the CPDT π-bridge of **C218** to give C═CPhCPDT (Fig. 1). We hypothesized that by introducing the extended conjugated system of C═CPhCPDT an increase in spectral response into the NIR region would be observed.[27]

Results and discussion

Two target dyes **YZ11** and **YZ13** directly replace the hexylchains of Hx_2CPDT with a simple phenyl-alkene. These dyes differ in orientation of the phenyl group either toward the acceptor (**YZ11**) or toward the donor (**YZ13**). Since alkyl chains often contribute to DSC device photovoltage increases, we also prepared two 3,5- or *meta*-dialkylated phenyl derivatives, **YZ16** and **YZ17**, which differ at the alkene conformation.

The synthesis of **YZ11**, **YZ13**, **YZ16** and **YZ17** proceeded in 5–7 steps from commercial materials (Scheme 1). The cross-conjugated

[a] Department of Chemistry and Biochemistry, University of Mississippi, University, MS 38677, USA. E-mail: delcamp@olemiss.edu
[b] School of Polymers and High Performance Materials, The University of Southern Mississippi, Hattiesburg, MS 39406, USA

† Electronic supplementary information (ESI) available. See DOI: 10.1039/c7cp06703h

‡ These authors contributed equally.

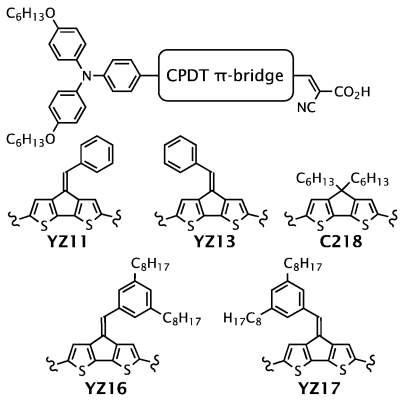

Fig. 1 Cross-conjugated C═CPhCPDT π-bridge based D–π–A dyes and **C218**.

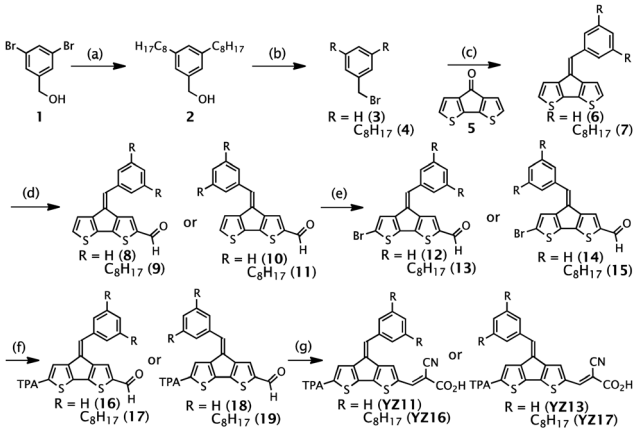

Scheme 1 Synthetic route to **YZ11**, **YZ13**, **YZ16** and **YZ17**. (a) Pd-PEPPSI-IPr (cat.), *n*-octylzinc bromide, 62%. (b) PBr_3, 73% (c) PPh_3, **5**, NaOEt, **6**: 76%, **7**: 60%. (d) $POCl_3$, DMF, **8**: 40%, **10**: 41%, **9**: 50%, **11**: 59%. (e) NBS, **12**: 96%, **14**: 100%, **13**: 95%, **15**: 91%. (f) TPA-Bpin, $Pd(PPh_3)_4$ (cat.), **16**: 91%, **18**: 69%, **17**: 100%, **19**: 83%. (g) Cyanoacetic acid, piperdine, **YZ11**: 87%, **YZ13**: 64%, **YZ16**: 20%, **YZ17**: 20%.

aryl group was synthesized *via* a Negishi coupling of dibromide **1**. Alcohol **2** was converted to the benzyl bromide **4** in high yield with the use of PBr_3. Next, either commercial benzyl bromide **3** or **4** was converted to a phosphonium salt and a Wittig reaction with 4*H*-cyclopenta[2,1-*b*:3,4-*b*′]dithiophen-4-one **5** gave the C═CPhCPDT substituted intermediates **6** and **7**, respectively. Vilsmeier–Haack reaction on **6** or **7** gave two silica gel column separable *E*/*Z* alkene isomers in equal ratios. The isomers were assigned *via* ^{1}H NMR NOE (nuclear Overhauser effect) experiments (Fig. 2). By irradiation of the proton on the CPDT ring adjacent to the aldehyde for isomers **8** and **10**, the two isomers could be differentiated. **10** shows a response from both the alkene proton and the aldehyde proton signaling that these protons are close enough for a through space interaction to be observed. This gave four separate C═CPhCPDT π-bridges, which smoothly underwent an NBS bromination, Suzuki coupling with TPABpin, and a Knoevenagel reaction to give **YZ11**, **YZ13**, **YZ16**, and **YZ17**.

UV-Vis absorption spectroscopy was performed with **YZ11**, **YZ13**, **YZ16**, **YZ17** and **C218** in dichloromethane to compare

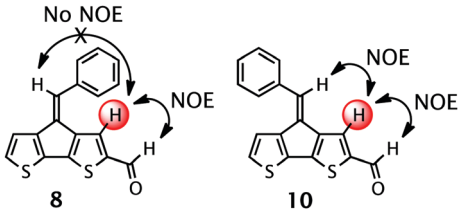

Fig. 2 NOE responses for **8** and **10**. Irradiated proton is highlighted in red.

changing the π-bridge from Hx_2CPDT to C═CPhCPDT (Fig. 3, top). The absorption maxima (λ_{max}) and absorption onsets (λ_{onset}) for all of the C═CPhCPDT dyes were red-shifted relative to **C218**. The molar absorptivities at λ_{max} for the C═CPhCPDT based dyes were measured to be very similar at 15 000 to 16 000 M^{-1} cm^{-1} (Table 1). This is slightly lower than **C218** at 20 000 M^{-1} cm^{-1}, however; a high-energy band near 440 nm for the cross-conjugated π-bridge based dyes reached molar absorptivities substantially higher than **C218** in this region. The C═CPhCPDT based panchromatic dyes show a much more even molar absorptivity across the full spectrum in solution than **C218**. Among the C═CPhCPDT based dyes, the octyl

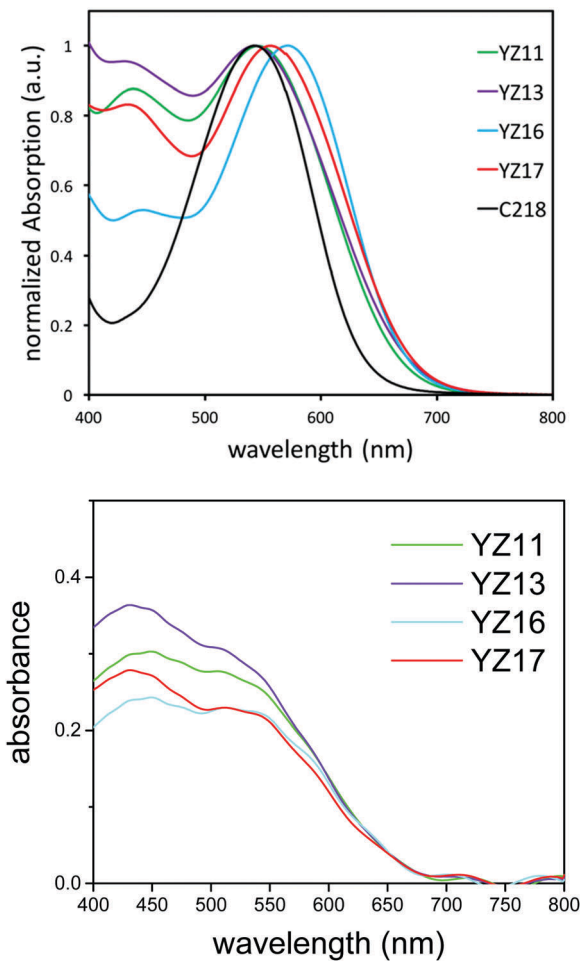

Fig. 3 UV-Vis absorption spectra collected for **YZ11**, **YZ13**, **YZ16**, **YZ17** and **C218** in CH_2Cl_2 at 25 °C (top) and on TiO_2 (bottom).

Table 1 Optical and electrochemical properties in CH_2Cl_2 at 25 °C[a]

Dye	λ_{onset} (nm)	λ_{max} (nm)	ε (M^{-1} cm^{-1})	$E_{(S+/S)}$ (V)	$E_{(S+/S^*)}$ (V)	E_g^{opt} (eV)
YZ11	675	546	15 000	0.87	−0.97	1.84
YZ13	690	553	15 000	0.89	−0.91	1.80
YZ16	690	572	16 000	0.89	−0.91	1.80
YZ17	690	557	16 000	0.93	−0.87	1.80
C218	630	550	20 000	0.89	−1.08	1.97

[a] See ESI for detailed energy measurements and calculations.

substituents on **YZ16** and **YZ17** led to slightly higher molar absorptivities than **YZ11** and **YZ13**. Interestingly, the dyes with the aryl groups oriented toward the donor region of the dye (**YZ13** and **YZ17**) have similar absorption spectra with the high energy region being higher in molar absorptivity than the dyes with the aryl groups oriented toward the acceptor. Dye–TiO_2 film UV-Vis absorption spectrum were also measured and are compared with the solution measurements as well as correlated to device performances below (Fig. 3, bottom).

Cyclic voltammetry was performed on **YZ11**, **YZ13**, **YZ16**, and **YZ17** to estimate the driving forces for electron transfer from the redox shuttle to the dye (ΔG_{reg}) and from the dye to the TiO_2 conduction band (ΔG_{inj}, Fig. 4). The ground-state oxidation potentials (0.87–0.93 V *versus* NHE) of these dyes were more positive than the I^-/I_3^- redox shuttle (0.35 V *versus* NHE), which favors electron transfer from I^- to the oxidized dye.[28,29] **YZ11**, **YZ13**, **YZ16**, **YZ17**, and **C218** have very similar $E_{(S+/S)}$ values, which indicate that the C═CPhCPDT bridge has minimal effects on ground-state state oxidation potential when compared with Hx_2CPDT. The excited-state oxidation potentials ($E_{(S+/S^*)}$) for **YZ11**, **YZ13**, **YZ16**, and **YZ17** were calculated from the equation $E_{(S+/S^*)} = E_{(S+/S)} - E_g^{opt}$ and were found to range from −0.87 to −0.97 V *versus* NHE which is suitable for efficient electron injection to the TiO_2 CB.[30] This is significantly lower in energy than the −1.08 V value measured for **C218**. The energetically lower $E_{(S+/S^*)}$ values for the cross-conjugated C═CPhCPDT bridge when compared to the Hx_2CPDT suggested that the excited-state is stabilized to a greater extent with the extended conjugation bridge with minimal effect on the ground-state oxidation potentials. This provides a valuable method for independently tuning dye redox potentials.

Having established **YZ11**, **YZ13**, **YZ16**, and **YZ17** as possessing suitable energetics to work efficiently in solar cell devices, we next evaluated the orbital position and involvement/electronic structure *via* density functional theory (DFT) and time-dependent density functional theory (TD-DFT) at the B3LYP/6-311G(d,p) level. For efficient DSC devices, the highest occupied molecular orbital (HOMO) of the dye should be oriented far from the TiO_2 surface to reduce the rate of back electron transfer from TiO_2 to the oxidized dye after an electron is injected. Also, the lowest unoccupied molecular orbital (LUMO) should be positioned near the TiO_2 surface to promote electron transfer upon photo-excitation. The HOMO and LUMO of **YZ17** are illustrated in Fig. 5 with the remaining dye orbitals available in the ESI† (Fig. S2). The HOMO is primarily located on the donor and CPDT portion of the π-bridge with some contribution on the CAA (cyanoacrylic acid) acceptor and no contribution on the cross-conjugated phenyl substituent. This is consistent with the CV data which suggests that there is minimal effect on the ground state oxidation potential by introducing the cross-conjugated phenyl substituent onto CPDT. The LUMO is positioned primarily on the CPDT-CAA region with some delocalization on the cross-conjugated phenyl substituent. The HOMO and LUMO of **YZ17** are well positioned for devices based on **YZ17** to operate efficiently. TD-DFT was performed for each dye to better understand the broad charge transfer bands observed in the absorption spectrum and the broad high energy bands (Table S1, ESI†). In each case, the HOMO–LUMO transition dominates the low-energy vertical transitions (96%), while both the HOMO−1 to LUMO (44%) and HOMO to LUMO+1 (51%) primarily contribute to the high-energy vertical transition. The HOMO−1 is delocalized across the entire dye with the exception of the cross-conjugated

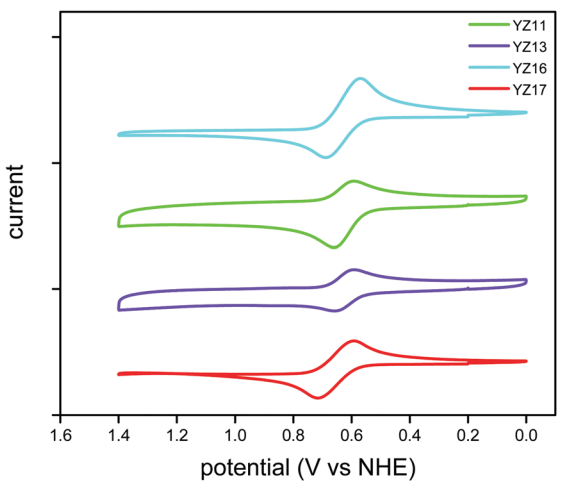

Fig. 4 Cyclic voltammograms for **YZ11**, **YZ13**, **YZ16**, and **YZ17** in CH_2Cl_2 with 0.1 M tetrabutylammonium hexafluorphosphate electrolyte, glassy carbon working electrode, platinum counter electrode and Ag/AgCl reference electrode.

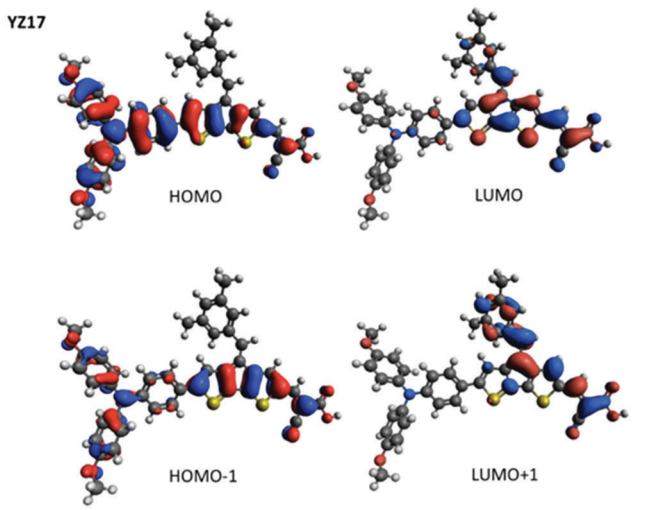

Fig. 5 HOMO, LUMO, HOMO−1, LUMO+1 orbitals for dye **YZ17** as calculated by DFT at B3LYP/6-311G(d,p) level.

phenyl substituent, and the LUMO+1 is entirely localized on the cross-conjugated phenyl substituent and cyanoacrylic acid regions. This result shows that the cross-conjugated phenyl substituent plays a critical role in influencing the LUMO and LUMO+1 resulting in strengthened high and low-energy charge transfer bands.

Solar cells were assembled and characterized according to the equation, PCE = $(J_{sc} \times V_{oc} \times FF)/I_0$ where PCE is power conversion efficiency, J_{sc} is the short circuit current, V_{oc} is the open circuit voltage, FF is the fill factor, and I_0 is the sun intensity. A range of PCE's were observed for devices prepared with **YZ11**, **YZ13**, **YZ16** and **YZ17** from 4.2% to 6.7% using the I^-/I_3^- redox couple (Table 2 and Fig. 6). The dialkylated C═CPhCPDT bridged dyes **YZ16** and **YZ17** gave higher open circuit voltages (622 and 671 mV, respectively) than the non-alkylated C═CPhCPDT bridged dyes **YZ11** and **YZ13**. For the dyes with the phenyl substituent oriented toward the acceptor (**YZ11** and **YZ16**), similar overall PCE values of 5.4% *versus* 5.1% were obtained, respectively, with a higher photocurrent observed for **YZ11**. A significant difference in PCE was observed for devices prepared with **YZ13** and **YZ17**, which have the phenyl substituent oriented toward the donor (4.2% *versus* 6.7%). This performance enhancement was the result of significant gains to both photocurrent and photovoltage for **YZ17** to give the highest performing dye of the series. Under identical device conditions, **YZ17** has a higher PCE than benchmark dye **C218** due to the panchromatic absorption of **YZ17** with a peak incident photon-to-current conversion efficiency (IPCE) of 67% and an IPCE onset of 800 nm (Fig. 6). This broadened IPCE response translates into a high J_{sc} of 13.6 mA cm^{-2} for **YZ17** compared to 13.2 mA cm^{-2} for **C218**. The V_{oc} and J_{sc} of **YZ17** could be enhanced to give a 7.6% PCE device through the use of N_2 bubbling during electrode sensitization to accelerate dye infiltration throughout the TiO_2 film. The peak IPCE for this device reaches 77%, although the IPCE spectrum onset is blue-shifted by approximately 20 nm relative to the **YZ17**-based electrodes prepared without gas flow a higher J_{sc} value of 14.7 mA cm^{-2} is obtained.

Table 2 Photovoltaic parameters of devices[a]

Dye	V_{oc} (mV)	J_{sc} (mA cm^{-2}) [IPCE J_{sc}][b]	FF	PCE (%)
YZ11	599	12.9 [12.5]	0.67	5.4
YZ13	577	9.8 [9.4]	0.72	4.2
YZ16	622	12.3 [11.8]	0.65	5.1
YZ17	671	13.6 [13.4]	0.71	6.7
YZ17[c]	683	14.7 [13.5]	0.74	7.6
C218	654	13.2 [12.6]	0.70	6.3

[a] The electrolyte is composed of guanadinium thiocyanate (GuNCS, 0.1 M), 1,3-dimethylimidazolium iodide (DMII, 1.0 M), I_2 (0.03 M), 4-*tert*-butyl pyridine (TBP, 0.5 M), LiI (1.0 M), and MeCN : valeronitrile (85 : 15) as solvent unless otherwise noted. The electrodes were dipped in 0.3 mM acetonitrile : *tert*-butanol : THF (1 : 1 : 1) with 20× CDCA overnight. [b] Calculated by integrating the area under the IPCE curves in Fig. 6. [c] **YZ17** dipping in acetonitrile : *tert*-butanol : chlorobenzene (2.5 : 2.5 : 1) dye solution with N_2 passed over the dye solution for 30 minutes. Measurements were carried out under simulated 1 Sun illumination (100 mW cm^{-2}), with active area of 0.15 cm^2 for the cells. Standard deviations are reported in the ESI (Table S4).

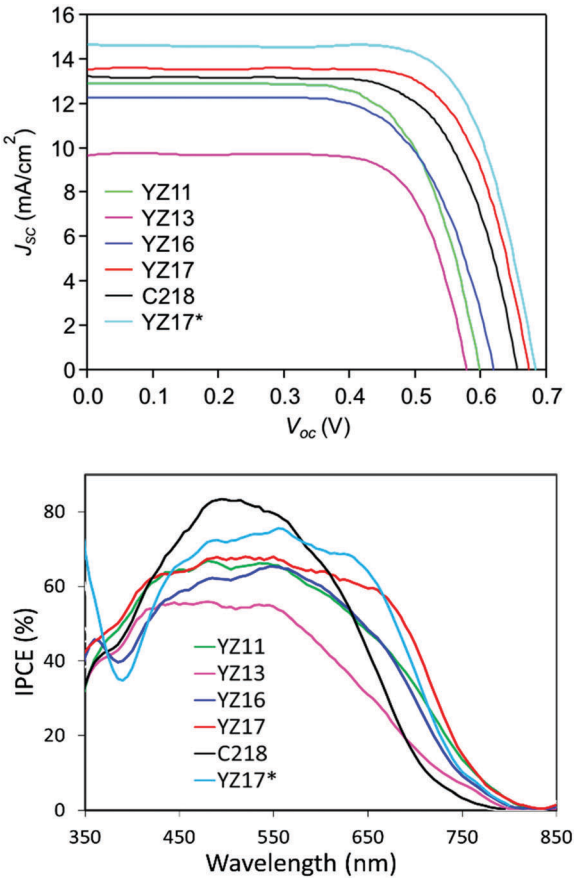

Fig. 6 *J*–*V* curves (top) and IPCE (bottom) for DSC devices of **YZ11**, **YZ13**, **YZ16**, **YZ17**, and **C218**. * Electrode was sensitized during N_2 bubbling.

Comparing phenyl group orientation with device performance, the non-alkylated phenyl group oriented toward the acceptor (*E*-isomer, dye **YZ13**) is higher performing by 1.2% PCE. However, for the heavily alkylated phenyls the phenyl group pointed toward the donor (*Z*-isomer, dye **YZ17**) is higher performing by 1.6% PCE. We reasoned the bulky chain alkylated phenyl group of *E*-isomer **YZ16** could result in a lower dye loading due to sterics near the surface. Dye loading studies reveal this is the case as **YZ17** has a nearly 2× higher dye loading on the TiO_2 surface (2.1×10^{-8} *versus* 3.7×10^{-8} mol cm^{-2}, Table S3, ESI†). **YZ13** with the smaller phenyl group oriented away from the surface only shows a modestly higher dye loading than **YZ11** (4.6×10^{-8} *versus* 3.9×10^{-8} mol cm^{-2}). This suggests that if the dye loadings are similar, the phenyl group oriented toward the surface is higher performing (*E*-isomer **YZ11** > *Z*-isomer **YZ13** in terms of PCE). However, if the phenyl group near the surface has significant steric bulk, the dye loading is significantly diminished and the phenyl group oriented away from the surface will be higher performing (*Z*-isomer **YZ17** > *E*-isomer **YZ16** in terms of PCE). Analysis of the film absorption compared to solution absorption reveals a substantial increase in the high energy absorption band of the film (relative to solution) for the donor oriented phenyl groups (*Z*-isomer dyes **YZ13** and **YZ17**). This significant change could suggest either the dye planarity has

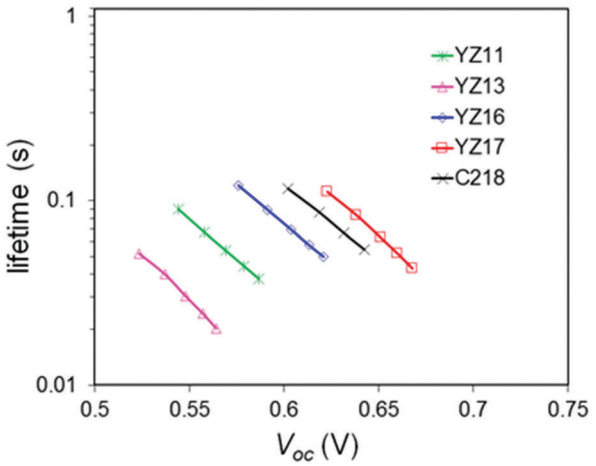

Fig. 7 Electron lifetime *versus* open-circuit voltage plot.

changed at the surface significantly or the *Z*-isomers are more prone to aggregation. For the smaller non-alkylated phenyl group, we observe a correlation between keeping the solution curve shape with film measurements and high performance. However, this gain in performance is offset if the dye loadings are not similar as observed for the alkylated phenyl group dyes.

Electron lifetime studies were undertaken to better understand the higher V_{oc} values observed for the alkylated C═CPhCPDT bridged dyes *versus* the non-alkylated dyes and the higher V_{oc} values observed for **YZ17** relative to **C218** for devices prepared under identical conditions (Fig. 7). A decrease in electron lifetimes was observed across the series in the following order: **YZ17** > **C218** > **YZ16** > **YZ11** > **YZ13**, which is identical to the order observed for the device V_{oc} values. This suggests the long alkyl chains of **YZ17** oriented away from the surface are most effective at reducing the rate of recombination of electrons in TiO_2 with the redox shuttle. The broadened absorption and longer lifetime of electrons in TiO_2 of **YZ17** illustrate the utility of a cross-conjugated CPDT bridge relative to the commonly used Hx_2CPDT building block.

Conclusion

Four cross-conjugated CPDT-based organic sensitizers were designed and synthesized. Dye isomers were assigned based on ^{1}H NMR NOE studies, and the dyes were characterized *via* UV, CV, and computational studies to probe the effects of a cross-conjugated π-bridge on dye energetics. The C═CPhCPDT bridge leads to a red-shift of the absorption spectrum and an increase in the high-energy absorption to give a series of panchromatic dyes. The red-shift in the absorption spectrum was found to be due to a stabilization of the dye excited-state oxidation potential. The addition of long alkyl chains onto the cross-conjugated CPDT bridge oriented away from the TiO_2 surface was found to reduce recombination of electrons in TiO_2 with the oxidized redox shuttle. A peak PCE of 7.6% was observed for **YZ17**, which surpasses the benchmark **C218** under identical device conditions. This performance enhancement was in part due to an extended IPCE range reaching an 800 nm onset for **YZ17**. The cross-conjugated CPDT bridge approach offers a new strategy for tuning dye energetics to increase light absorption and increase device performance relative to the ubiquitous Hx_2CPDT bridge used in **C218**.

Conflicts of interest

There are no conflicts to declare.

Acknowledgements

YZ, HC, AM and JHD thank NSF for a CAREER Award 1455167. AM and JHD thank the NSF REU Award 1460568. AEL and JDA are grateful for support from the National Science Foundation (NSF OIA-1632825 and DGE-1449999).

Notes and references

1 S. Zhang, X. Yang, Y. Numata and L. Han, *Energy Environ. Sci.*, 2013, **6**, 1443–1464.
2 B. O'Regan and M. Grätzel, *Nature*, 1991, **353**, 737–740.
3 D. Butler, *Nature*, 2008, **454**, 558–559.
4 B. P. Jelle and C. Breivik, *Energy Procedia*, 2012, **20**, 78–87.
5 A. Fakharuddin, R. Jose, T. M. Brown, F. Fabregat-Santiago and J. Bisquert, *Energy Environ. Sci.*, 2014, **7**, 3952–3981.
6 S. Mathew, A. Yella, P. Gao, R. Humphry-Baker, B. F. Curchod, N. Ashari-Astani, I. Tavernelli, U. Rothlisberger, M. K. Nazeeruddin and M. Grätzel, *Nat. Chem.*, 2014, **6**, 242–247.
7 K. Kakiage, Y. Aoyama, T. Yano, T. Otsuka, T. Kyomen, M. Unno and M. Hanaya, *Chem. Commun.*, 2014, **50**, 6379–6381.
8 K. Kakiage, Y. Aoyama, T. Yano, K. Oya, T. Kyomen and M. Hanaya, *Chem. Commun.*, 2015, **51**, 6315–6317.
9 K. Kakiage, Y. Aoyama, T. Yano, K. Oya, J. I. Fujisawa and M. Hanaya, *Chem. Commun.*, 2015, **51**, 15894–15897.
10 P. Gao, H. N. Tsao, C. Yi, M. Grätzel and M. K. Nazeeruddin, *Adv. Energy Mater.*, 2014, **4**, 1301485.
11 T. W. Holcombe, J. H. Yum, J. Yoon, P. Gao, M. Marszalek, D. Di Censo, K. Rakstys, M. K. Nazeeruddin and M. Grätzel, *Chem. Commun.*, 2012, **48**, 10724–10726.
12 J. H. Yum, T. W. Holcombe, Y. Kim, J. Yoon, K. Rakstys, M. K. Nazeeruddin and M. Grätzel, *Chem. Commun.*, 2012, **48**, 10727–10729.
13 Z. Yao, H. Wu, Y. Li, J. Wang, J. Zhang, M. Zhang, Y. Guo and P. Wang, *Energy Environ. Sci.*, 2015, **8**, 3192–3197.
14 Y. Ooyama and Y. Harima, *ChemPhysChem*, 2012, **13**, 4032–4080.
15 J. H. Delcamp, A. Yella, M. K. Nazeeruddin and M. Grätzel, *Chem. Commun.*, 2012, **48**, 2295–2297.
16 M. Zhang, Y. Wang, M. Xu, W. Ma, R. Li and P. Wang, *Energy Environ. Sci.*, 2013, **6**, 2944–2949.
17 A. Yella, H. W. Lee, H. N. Tsao, C. Yi, A. K. Chandiran, M. K. Nazeeruddin, E. W. Diau, C. Y. Yeh, S. M. Zakeeruddin and M. Grätzel, *Science*, 2011, **334**, 629–634.
18 A. J. Huckaba, A. Yella, P. Brogdon, J. Scott Murphy, M. K. Nazeeruddin, M. Grätzel and J. H. Delcamp, *Chem. Commun.*, 2016, **52**, 8424–8427.

19 H. Cheema and J. H. Delcamp, *ACS Appl. Mater. Interfaces*, 2017, **9**, 3050–3059.
20 A. Mishra, M. K. Fischer and P. Bäuerle, *Angew. Chem., Int. Ed.*, 2009, **48**, 2474–2499.
21 A. Hagfeldt, G. Boschloo, L. Sun, L. Kloo and H. Pettersson, *Chem. Rev.*, 2010, **110**, 6595–6663.
22 S. Ahmad, E. Guillén, L. Kavan, M. Grätzel and M. K. Nazeeruddin, *Energy Environ. Sci.*, 2013, **6**, 3439.
23 Z. Sun, M. Liang and J. Chen, *Acc. Chem. Res.*, 2015, **48**, 1541–1550.
24 J.-H. Yum, E. Baranoff, S. Wenger, M. K. Nazeeruddin and M. Grätzel, *Energy Environ. Sci.*, 2011, **4**, 842–857.
25 R. Li, J. Liu, N. Cai, M. Zhang and P. Wang, *J. Phys. Chem. B*, 2010, **114**, 4461–4464.
26 H. Wang, M. Liu, M. Zhang, P. Wang, H. Miura, Y. Cheng and J. Bell, *Phys. Chem. Chem. Phys.*, 2011, **13**, 17359–17366.
27 A. E. London, L. Huang, B. A. Zhang, M. B. Oviedo, J. Tropp, W. Yao, Z. Wu, B. M. Wong, T. N. Ng and J. D. Azoulay, *Polym. Chem.*, 2017, **8**, 2922–2930.
28 G. Boschloo and A. Hagfeldt, *Acc. Chem. Res.*, 2009, **42**, 1819–1826.
29 A. Y. Anderson, P. R. F. Barnes, J. R. Durrant and B. C. O'Regan, *J. Phys. Chem. C*, 2011, **115**, 2439–2447.
30 A. Listorti, B. O'Regan and J. R. Durrant, *Chem. Mater.*, 2011, **23**, 3381–3399.

